Computational Biology and Chemistry 120 (2026) 108763

Contents lists available at ScienceDirect

Computational Biology and Chemistry

journal homepage: www.elsevier.com/locate/cbac

Searching for potential xanthine oxidase inhibitors from *Vietnamese* herb plants via computational studies

Anh Hung Nguyen [a,1], Anh Tuan Do [b,c,1], Nguyen Ngoc Linh [d], Minh Quan Pham [e,f], Son Tung Ngo [b,c], Thi-Kim-Dung Le [b,c,*]

[a] Faculty of Chemistry, Hanoi Pedagogical University 2, Phu Tho, Vietnam
[b] Laboratory of Biophysics, Institute for Advanced Study in Technology, Ton Duc Thang University, Ho Chi Minh City, Vietnam
[c] Faculty of Pharmacy, Ton Duc Thang University, Ho Chi Minh City, Vietnam
[d] Faculty of Pharmacy, Thanh Do University, Kim Chung, Hoai Duc, Hanoi, Vietnam
[e] Institute of Chemistry, Vietnam Academy of Science and Technology, Hanoi, Vietnam
[f] Graduate University of Science and Technology, Vietnam Academy of Science and Technology, Hanoi, Vietnam

ARTICLE INFO

Keywords:
Xanthine oxidase
Vietnamese herbs
Molecular docking
MM-PBSA

ABSTRACT

Gout, a prevalent form of inflammatory arthritis, affects individuals of all ages and is increasing worldwide. It is closely associated with hyperuricemia, a condition caused by excessive uric acid production. Xanthine oxidase (XO) inhibitors play a key role in managing hyperuricemia, making the discovery of new and effective inhibitors a priority in drug development. In this study, computational methods were employed to screen natural compounds for their potential to inhibit XO. A total of 4947 compounds derived from 71 Vietnamese medicinal herbs were subjected to molecular docking simulations, leading to the identification of eight candidates with strong binding affinities and favorable drug-likeness according to Lipinski's rule. To further validate these findings, molecular dynamics (MD) simulations and molecular mechanics Poisson–Boltzmann surface area (MM-PBSA) calculations were performed. Five newly discovered compounds, namely salvianolic acid A, puerarol, ochnaflavone, and forsythensides A and B, showed lower predicted binding energies than topiroxostat, suggesting their potential for further exploration as putative XO inhibitors. Notably, Van der Waals forces predominated over electrostatic interactions in the binding of these top candidates. The residues Glu802, Arg880, Thr1010, and Glu1261 served as key contributors to ligand binding, forming strong hydrogen bonds and side-chain contacts with the inhibitors. These findings offer valuable mechanistic insights into the interaction between natural compounds and XO, and highlight potential candidates for the development of novel XO inhibitors.

1. Introduction

Gout, an inflammatory form of arthritis, is not limited by gender or age and is increasingly prevalent on a global scale. Globally, gout prevalence has been estimated to be between 0.1 % and 10 % on average (Kuo et al., 2015). In Vietnam, specifically in the capital city of Hanoi, which houses nearly 8 million residents, the prevalence of gout stands at approximately 0.14 %, as reported by the Community Oriented Program for the Control of Rheumatic Diseases (COPCORD) (Minh Hoa et al., 2003). This disease is characterized by persistently elevated levels of uric acid in the blood (Masseoud et al., 2005). This elevation prompts the formation of monosodium urate crystals, which can accumulate in synovial fluid or neighboring tissues, leading to episodes of acute and chronic inflammation, tissue deterioration, and discomfort (Pascart and Lioté, 2018).

In humans, the final byproduct of dietary and endogenous purines is uric acid (Ishikawa et al., 2013). The linked metabolic pathway is made up of several stages of reactions that are facilitated by various enzymes, such as xanthine oxidase (XO), purine nucleoside phosphorylase, and adenosine deaminase (Pedley and Benkovic, 2017). Among these, the transformation of hypoxanthine into xanthine and xanthine into uric acid is catalyzed by XO (Gliozzi et al., 2016; Ojha et al., 2016). Drug development studies have mostly focused on the role of XO inhibition in lowering uric acid levels, and XO inhibitors constitute the cornerstone of

* Corresponding author at: Laboratory of Biophysics, Institute for Advanced Study in Technology, Ton Duc Thang University, Ho Chi Minh City, Vietnam.
E-mail address: dung.lethikim@tdtu.edu.vn (T.-K.-D. Le).
[1] These authors contributed equally to this work and share first authorship

https://doi.org/10.1016/j.compbiolchem.2025.108763
Received 14 September 2025; Received in revised form 1 November 2025; Accepted 3 November 2025
Available online 4 November 2025

treatment for reducing blood urate levels in patients with gout or hyperuricemia (Pascart and Lioté, 2018; Song et al., 2023). However, current XO-inhibiting drugs still have many side effects, which could be fatal in some cases (Bayat et al., 2016; Cicero et al., 2021).

Although synthetic chemistry is currently receiving significant attention as the main method to discover and produce drugs, the role of plants in treating and preventing diseases remains substantial. Compounds derived from plants have long been used as medicine to treat a variety of diseases, and patients are likely to tolerate and accept them better. About 70,000 plant species have been investigated for potential medical use so far (Veeresham, 2012). According to Zhang et al., 80 % of 122 drugs derived from plants were associated with their original ethnopharmacological applications (Zhang et al., 2020). Notably, Vietnam has a rich tradition of herbal medicine, which remains closely integrated with modern medical practices. Many officially registered pharmaceutical products containing herbal ingredients are currently used alongside conventional treatments. This longstanding tradition highlights the potential of Vietnamese medicinal plants as promising sources for alternative therapies with fewer adverse effects.

Traditional drug discovery methods are typically expensive and time-consuming. Currently, with the support of computer-aided drug design, discovering new inhibitors to prevent the biological activity of enzymes has been significantly accelerated (Alonso et al., 2006; Marshall, 1987; Sliwoski et al., 2014; Van Drie, 2007). In particular, the ligand-binding affinity is considered using various approaches (Ngo, 2021; Pham et al., 2021; Ryde and Soderhjelm, 2016), and the pharmacokinetics are probed via calculation of absorption, distribution, metabolism, excretion, and toxicity (Chhetri et al., 2021; Lee et al., 2003). Normally, the molecular docking and molecular dynamics simulations are employed to clarify both ligand-binding free energy and the mechanism of the ligand-binding process (Nguyen et al., 2022; Tam et al., 2023; Thai et al., 2024).

Therefore, to identify new XO inhibitors from natural products for the treatment of hyperuricemia and gout, we employed a high-throughput virtual screening strategy integrating molecular docking with Molecular Mechanics Poisson–Boltzmann Surface Area (MM-PBSA) calculations. Initially, the most suitable docking protocol and rationale were determined through re-docking validation. Subsequently, docking analyses were performed on 4947 natural compounds derived from 71 Vietnamese medicinal plants, and their binding affinities were further evaluated using MM-PBSA. This study represents the first systematic screening of natural compounds from Vietnamese medicinal plants for their anti-XO activity using an integrated computational approach. By comparing the binding affinities of hit compounds with reference drugs (topiroxostat and febuxostat), we identified salvianolic acid A, puerarol, ochnaflavone, and forsythensides A and B as newly discovered compounds with potential XO inhibitory activity. These results provide valuable insights into their interaction patterns within the XO active site and establish a foundation for future experimental validation.

2. Materials and methods

2.1. Structure of xanthine oxidase and its ligands

Eight experimental structures of *Bos taurus* xanthine oxidase (XO) in complex with co-crystallized ligands were obtained from the RCSB Protein Data Bank (PDB IDs: 1FIQ (Enroth et al., 2000), 3B9J (Pauff et al., 2008), 3ETR (Pauff et al., 2009), 3NRZ (Cao et al., 2010), 3NS1 (Cao et al., 2010), 3NVW (Cao et al., 2014a), 3NVY (Cao et al., 2014b), and 3NVZ (Cao et al., 2014a)). Sequence comparison of XO proteins was performed using the online tool provided by VectorBuilder (https://vectorbuilder.com), with the structure 3NRZ chosen as the reference due to its complex with hypoxanthine, the natural substrate of XO. Systems exhibiting sequence similarity greater than 99 % with the reference were selected for molecular docking.

Structures of eight experimental ligands used for method validation were retrieved from the PubChem database (Kim et al., 2016). Additionally, the details of compounds derived from 71 Vietnamese medicinal herbs were collected from the database provided in the Supporting Information.

2.2. Molecular docking simulations

Molecular docking simulations were performed using four scoring functions: AutoDock Vina 1.2 (vina), AutoDock4 (ad4), Vinardo, and mVina (a modified version of AutoDock Vina) (Pham et al., 2021). Protein structures, co-crystallized ligands, and grid box files were prepared using AutoDockTools, with polar hydrogens and partial atomic charges added. The grid box was defined with dimensions of $20 \times 20 \times 20$ Å to fully cover the active site located on chain C of the XO structures. Exhaustiveness values of 8 and 56 were tested to evaluate method convergence.

Root mean square deviations (RMSDs) between co-crystallized ligands and redocked poses were calculated using the Zhanglab online tool. A threshold of RMSD < 0.2 nm was applied to determine successful docking rates, thereby assessing the reliability of each scoring function. Experimental IC_{50} values of the selected inhibitors were obtained from the literature. For receptor-based validation, PDB ID 3NVW was employed. Correlation analysis between docking scores and experimental data was carried out using the mVina scoring function with exhaustiveness $= 8$. Pearson's correlation coefficients (R) and associated errors were estimated by a bootstrapping approach through 1000 loops.

2.3. Molecular dynamics simulations

Molecular dynamics (MD) simulations were performed using the GROMACS 2019.6 package (Abraham et al., 2015) to investigate the ligand-binding process to XO. The protein, ions, and water molecules were parameterized with the Amber99SB-iLDN force field (Aliev et al., 2014), and the TIP3P model is used for water molecules, following previously published protocols (Zhang et al., 2018b, 2018c). Quantum chemical calculations, based on Density Functional Theory (DFT) calculations with the double hybrid B3LYP functional at the level of 6–31 G (d,p) basis set, were carried out to determine the optimized geometry and atomic charges of each ligand. The ligands were further parameterized using the General Amber Force Field (GAFF) (Wang et al., 2004) in combination with AmberTools23 (Case et al., 2023) and ACPYPE (Sousa da Silva and Vranken, 2012) to change the format from Amber to GROMACS (Abraham et al., 2015). The resulting protein–ligand complexes were solvated in a dodecahedral periodic boundary condition (PBC) box of 1444.0 nm^3 , ensuring 1.2 nm between the complex and the boundaries, and containing approximately 143,000 atoms.

MD simulations protocols followed established parameters (Ngo, 2022; Nguyen et al., 2025; Thai et al., 2022). The integration step was set to 3 fs, and nonbonded interactions were computed with a cutoff of 9.0 Å. Electrostatic and van der Waals (vdW) interactions were treated with the Particle-Mesh Ewald (PME) method (Darden et al., 1993) and cut-off schemes, respectively. The LINCS algorithm was applied to constrain all bonds in simulations with an order of 4. Each solvated complex underwent energy minimization by the steepest descent method, followed by equilibration under NVT and NPT ensembles (100 ps each) with 1000 kJ mol^{-1} nm^{-2} positional restraints to all heavy atoms. Reference temperature and pressure were set to 310 K and 1 bar, respectively. Subsequently, unbiased MD simulations were performed for 200 ns. To ensure adequate sampling, all simulations were repeated in triplicate. During MD simulations, systemic coordinates were recorded every 100 ps.

Trajectory analyses were conducted with GROMACS tools. Root mean square deviation (RMSD) and radius of gyration (R_g) were calculated to assess the structural stability of protein–ligand complexes. Hydrogen bonds (HBs) and side-chain contacts (SCs) were analyzed to characterize ligand interactions with key active-site residues of XO.

Electrostatic surface maps of protein–ligand complexes were generated using the APBS plugin in PyMOL to further probe binding conformations.

2.4. MM-PBSA

MM-PBSA calculations were performed using g-mmpbsa (Kumari et al., 2014), a computational tool developed on top of two open-source software packages, GROMACS and APBS. For Poisson–Boltzmann (PB) calculations, the coarse grid and fine grid sizes were set with parameters *cfac* = 1.5 and *fadd* = 5, respectively, using a grid spacing of 0.5 Å. In the polar solvation calculation, the solute dielectric constant ε_{solute} was set to 2, with vacuum (vdie) and solvent (sdie) dielectric constants set to 1 and 80, respectively. Solvent probe radius (srad) was 1.4 Å and the LPBE solver was used. For the non-polar calculation, SASA model was used with a probe radius (sasrad) of 1.4 Å, and a surface tension coefficient γ of 0.00542 kcal $mol^{-1}Å^{-2}$.

The total binding free energy ($\Delta G_{MM\text{-}PBSA}$) is determined by combining three main components: the gas-phase interaction energy between the ligand and protein (ΔE_{MM}), the solvation free energy difference (ΔG_{sol}), and the entropic contribution arising from conformational changes upon binding (−TΔS). The formulation is displayed as follows:

$$\Delta G_{MM\text{-}PBSA} = \Delta E_{MM} + \Delta G_{sol}$$

where $\Delta E_{MM} = \Delta E_{cou} + \Delta E_{vdw}$ and $\Delta G_{sol} = \Delta G_{sur} + \Delta G_{PB}$

The ΔE_{cou} and ΔE_{vdw} are the electrostatic and van der Waals energy of complexes, while ΔG_{sur} and ΔG_{PB} are non-polar and polar energy, respectively. Besides, the entropic term (–TΔS) was not computed in this work due to its high computational consumption and less accuracy with a large complex, which is a common usage in MM-PBSA analysis for virtual screening (He et al., 2024; Liu et al., 2025; Pan et al., 2021; Wang et al., 2001; Wang and Kollman, 2001).

2.5. ADME

To predict ADME, we used the website PreADMET (S.K.Lee, 2004).

2.6. Analyzed tools

The protonation states of ligands were calculated by the online tool Chemicalize (https://chemicalize.com). The MD-refined structures were obtained via the clustering method (Abraham et al., 2015). The intermolecular contact between a ligand and protein was probed via PyMOL (Schrödinger LLC, 2010) and Maestro free version (Schrödinger LLC, 2020).

3. Results and discussion

3.1. Docking simulations

Molecular docking was first developed in the 1980s, and since then, numerous docking programs have been created, primarily to investigate protein–ligand interactions in the context of drug discovery (Kuntz et al., 1982). However, docking programs continue to face limitations, particularly in modeling protein flexibility, incorporating solvation effects, and accurately estimating binding affinities (Huang and Zou, 2010; Kolb and Irwin, 2009). Previous studies have shown that the docking success rate depends on many factors, one of which is the target being investigated (Warren et al., 2006). Therefore, we first determine the most suitable docking method for XO by determining the docking success rate. Eight co-crystallized structures of *Bos taurus* xanthine oxidase were retrieved from the RCSB database (PDB IDs: 1FIQ, 3B9J, 3ETR, 3NRZ, 3NS1, 3NVW, 3NVY, and 3NVZ), and those with sequence similarity greater than 99 % were selected for re-docking (see Table S1, Supporting Information). Simulations were conducted using four different scoring functions, including vina (Trott and Olson, 2010), ad4 (Morris et al., 2009), vinardo (Quiroga and Villarreal, 2016), and mVina (Pham et al., 2021). The root-mean-square deviation (RMSD) was used as the evaluation parameter, and an RMSD value below 0.2 nm indicates a valid docking protocol suitable for further docking studies (Bell and Zhang, 2019). In addition, exhaustiveness refers to the number of initial random searches performed for ligand conformation exploration and optimization, with a default value of 8 in Vina due to confirmation of previous benchmarks (Nguyen et al., 2020; Pham et al., 2021). Overall, increasing the exhaustiveness improves the thoroughness of the conformational space search within the protein structure, but it also increases computational cost. In this work, we evaluated the docking results at exhaustiveness levels of 8 and 56, with the outcomes presented in Tables 1 and 2 and in Fig. 1. As shown in Fig. 1, mVina achieved the highest docking success rate (63 %), with no difference between the two exhaustiveness settings. Therefore, mVina with an exhaustiveness of 8 was selected as the optimal condition for molecular docking to identify potential XO inhibitors. The docking pose is shown in Tables S2 and S3, Supporting Information.

We further evaluated the docking performance on XO by analyzing the binding energies of eight available inhibitors, using the above-determined docking conditions and the receptor 3NVW (Cao et al., 2014a), which has the highest resolution (1.6 Å) and has also been employed in an earlier study (Pan et al., 2021). The outcomes are displayed in Table 3 and Table S4. The computed binding free energy via mVina (Table 3) showed good agreement with the respective experimental results, as evidenced by the correlation coefficient $R = 0.79 \pm 0.14$ (cf. Fig. 2). This consistency demonstrates that mVina can be used for ranking the ligand-binding affinity of the XO target.

3.1.1. Docking results of 71 Vietnamese herbs

A total of 4947 natural compounds from 71 Vietnamese herbs were screened to identify potential inhibitors for XO using AutoDock Vina with modified empirical parameters. Lipinski's "rule of five" helps to predict whether a biologically active compound possesses the physicochemical characteristics required for oral bioavailability (Lipinski, 2004). We applied this rule to filter the docking results, and eight compounds formed strong binding to XO and satisfied the criteria were identified, with the outcomes summarized in Table 4.

The binding affinity of top lead compounds ranged from −16.3 to −15.3 kcal mol^{-1}. Their ligand-binding poses were further analyzed, as shown in Fig. 3. Previous studies have demonstrated that the molybdopterin (Mo-pt) domain is the active site of XO, where xanthine is oxidized to uric acid, and is defined by key amino acids such as Asn768, Glu802, Leu873, Arg880, Phe1009, Thr1010, Val1011, and Glu1261 (Dong et al., 2016; Ghallab et al., 2022; Maguire et al., 2018; Ou et al., 2020). The results revealed that the top compounds were well accommodated in the active site and formed effective interactions with these critical residues. Such interactions altered the microenvironment and secondary structure of XO, leading to a reduction in its catalytic activity.

Table 1
RMSD of docking results with four scoring functions, exhaustiveness = 8.

No.	ID	RMSD mvina (nm)	RMSD vina1.2 (nm)	RMSD AD4 (nm)	RMSD vinardo (nm)
1	1FIQ	0.05	0.04	0.05	0.03
2	3B9J	0.04	0.38	0.36	0.38
3	3ETR	0.37	0.36	0.36	0.37
4	3NRZ	0.03	0.05	0.29	0.30
5	3NS1	0.26	0.36	0.36	0.36
6	3NVW	0.04	0.03	0.07	0.04
7	3NVY	0.84	0.71	0.32	0.70
8	3NVZ	0.15	0.12	0.11	0.10
	RMSD < 0.2 nm	63 %	50 %	38 %	38 %

Table 2
RMSD of docking results with four scoring functions, exhaustiveness = 56.

No.	ID	RMSD mvina (nm)	RMSD vina1.2 vina (nm)	RMSD vina1.2 ad4 (nm)	RMSD vina1.2 vinardo (nm)
1	1FIQ	0.05	0.02	0.05	0.03
2	3B9J	0.04	0.38	0.36	0.38
3	3ETR	0.37	0.36	0.36	0.37
4	3NRZ	0.03	0.05	0.29	0.30
5	3NS1	0.26	0.35	0.36	0.36
6	3NVW	0.03	0.04	0.07	0.04
7	3NVY	0.74	0.74	0.30	0.70
8	3NVZ	0.15	0.13	0.04	0.10
	RMSD < 0.2 nm	63 %	50 %	38 %	38 %

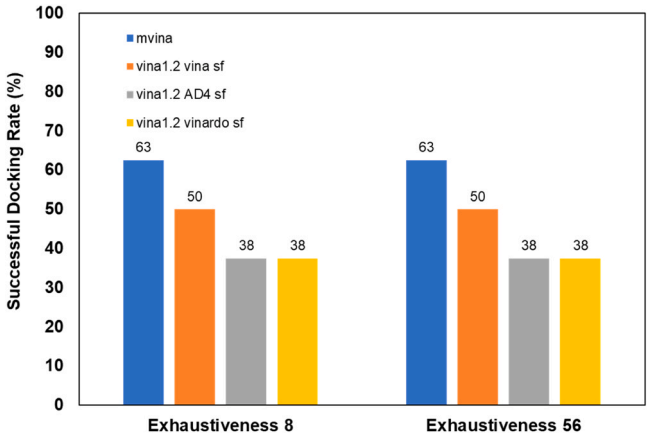

Fig. 1. Docking success rate of four scoring functions.

Table 3
The data from docking simulations and experiments of known inhibitors against XO.

No.	Ligand	IC_{50} (nm)	ΔG_{exp} (kcal/mol)	ΔG_{mvina} (kcal/mol)	Reference
1	topiroxostat	5.3	−11.4	−13.2	(Sato et al., 2009)
2	febuxostat	80	−9.7	−12.3	(Ghallab et al., 2022)
3	kaempferol	2180	−7.8	−12.1	(Wang et al., 2015)
4	quercetin	2740	−7.6	−12.6	(Zhang et al., 2018a)
5	baicalein	7540	−7.0	−11.8	(Zeng et al., 2018)
6	delphinidin−3-*O*-sambubioside	17100	−6.5	−10.4	(Xie et al., 2021)
7	GCG	33600	−6.1	−11.7	(Zhang et al., 2022)
8	pinobanksin	125100	−5.4	−11.1	(Dong et al., 2016)

The binding poses of the most promising compounds were then used as the initial conformations for MD simulations.

3.2. Molecular dynamics simulations

To evaluate conformational stability and assess the reliability of the MD simulations, the all-atom root mean square deviation (RMSD) was calculated (Table S5, Supporting Information). A small RMSD reflects a stable complex between the inhibitors and the XO protein. For the trajectories of XO bound to eight natural compounds and two reference inhibitors, febuxostat and topirostat, the RMSD reached equilibrium after approximately 100 ns of simulation, stabilizing around 0.3 nm. The RMSD results were consistent across triplicates, confirming that the systems are suitable for exploring the dynamic properties of the selected proteins. In addition, the rigidity of the protein system was evaluated using the radius of gyration (R_g) (Table S5, Supporting Information). The R_g, which measures the distribution of an object's mass around its axis of rotation, remained stable at approximately 2.88 nm for all eight complexes. This result indicates that the natural compounds induced only minimal structural perturbations, thereby preserving the overall integrity of XO.

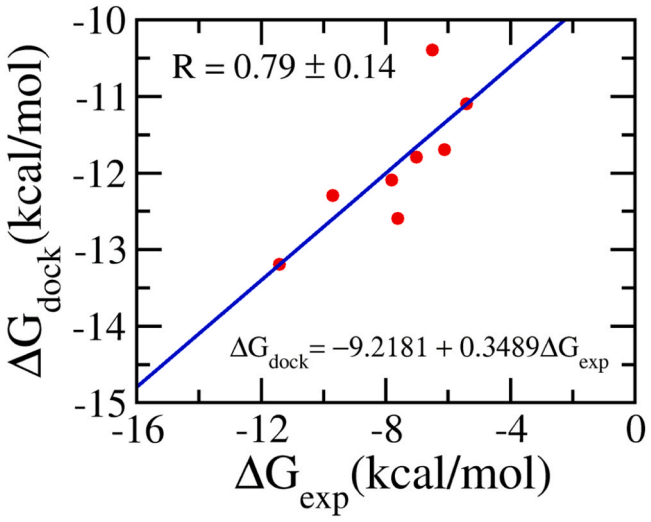

Fig. 2. Correlation coefficient between docking and experimental binding free energy of eight available inhibitors. Docking results were obtained *via* mVina application.

Table 4
Top-lead compounds predicted by mVina results for further calculations.

No.	Plants	Compound	ΔG_{mvina} (kcal mol^{-1})
1	*Forsythia suspensa*	forsythenside B	−16.3
2	*Lonicera japonica Thunb.*	ochnaflavone	−15.9
3	*Peucedanum decursivum Maxim.*	decursidate	−15.8
4	Salvia miltiorhiza / *Codonopsis pilosula*	salvianolic acid A	−15.6
5	*Pueraria thomsonii Benth*	puerarol	−15.4
6	*Forsythia suspensa*	forsythenside A	−15.3
7	*Angelica pubescens*	umbelliprenin	−15.3
8	*Orthosiphon aristatus*	(*R*)-(+)-rosmarinic acid	−15.3

3.3. MM-PBSA calculations

Although AutoDock Vina shows a good correlation with experimental data, docking programs generally rely on various approximations and constraints to accelerate the calculations. Consequently, validation of the docking results using more accurate, CPU-intensive approaches is necessary to ensure reliability (Nassar et al., 2023; Pan et al., 2021; Parihar et al., 2022). In this context, MM-PBSA has been widely employed to evaluate the binding affinity between ligands and XO in previous studies (Liu et al., 2025; Pan et al., 2021). Therefore, we also applied the MM-PBSA method in our work, which is based on the continuum model, as illustrated in Figure S1, Supporting Information.

The interaction energies, including van der Waals, electrostatic,

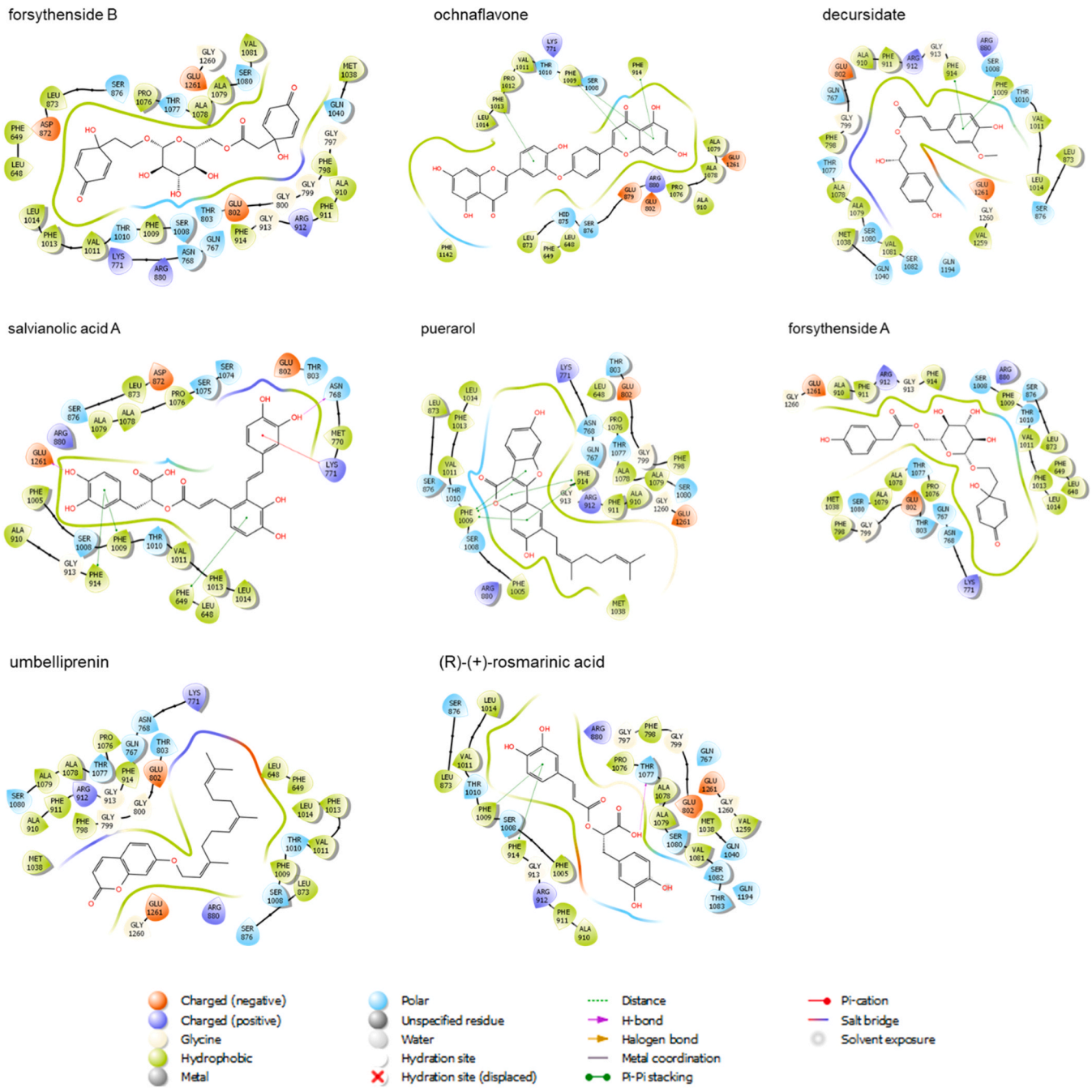

Fig. 3. The binding poses between 8 potential natural compounds and XO.

Table 5
MM-PBSA binding free energies of XO with 8 natural compounds and febuxostat, topiroxostat.

No.	Compound	ΔE_{vdw} kcal mol^{-1}	ΔE_{ele} kcal mol^{-1}	ΔG_{PB} kcal mol^{-1}	ΔG_{sur} kcal mol^{-1}	$\Delta G_{MM\text{-}PBSA}$ kcal mol^{-1}
1	salvianolic acid A	−37.83 ± 3.96	−149.07 ± 15.70	108.98 ± 6.85	−5.14 ± 0.24	−83.06 ± 13.14
2	(R)-(+)-rosmarinic acid	−46.77 ± 0.64	−108.44 ± 3.49	96.61 ± 1.60	−4.75 ± 0.02	−63.35 ± 1.85
3	puerarol	−61.14 ± 1.83	−38.65 ± 3.67	48.05 ± 2.64	−5.47 ± 0.02	−57.21 ± 0.33
4	ochnaflavone	−57.81 ± 2.20	−47.06 ± 6.96	57.11 ± 3.50	−5.80 ± 0.13	−53.57 ± 5.97
5	forsythenside A	−54.15 ± 1.96	−52.49 ± 4.48	62.32 ± 1.20	−5.72 ± 0.08	−50.03 ± 2.80
6	forsythenside B	−52.64 ± 2.81	−49.83 ± 14.24	59.71 ± 7.93	−5.54 ± 0.15	−48.30 ± 8.85
7	decursidate	−49.93 ± 0.87	−22.53 ± 1.40	43.39 ± 1.07	−4.74 ± 0.04	−33.80 ± 2.37
8	umbelliprenin	−39.99 ± 6.14	−11.14 ± 1.48	27.95 ± 5.80	−4.28 ± 0.61	−27.46 ± 2.30
9	febuxostat	−32.38 ± 3.20	−110.85 ± 1.75	72.20 ± 1.47	−3.93 ± 0.22	−74.96 ± 1.96
10	topiroxostat	−36.85 ± 0.32	−53.63 ± 2.80	53.70 ± 1.67	−3.33 ± 0.01	−40.11 ± 1.07

polar solvation, SASA, and overall binding energies, were calculated over the last 100 ns of the MD trajectory and are presented in Table 5. In this context, the currently used drugs topiroxostat and febuxostat served as a reference. The results showed that the average binding energies of salvianolic acid A, rosmarinic acid, puerarol, ochnaflavone, and forsythensides A and B, ranging from –48.30 to –83.06 kcal mol^{-1}, were lower than that of topiroxosat ($\Delta G_{MM\text{-}PBSA}$ = −40.11 ± 1.07 kcal mol^{-1}). This finding suggests that these natural compounds strongly bind to XO due to their high van der Waals interactions. For all six systems, ΔE_{vdw} contributed predominantly to $\Delta G_{MM\text{-}PBSA}$, while the electrostatic energy (ΔE_{ele}) was nearly counteracted by the polar solvation term (ΔG_{PB}). In contrast, the solvation free energy from the solvent-accessible surface area (ΔG_{sur}) was comparable across the complexes. Collectively, these results indicate that nonpolar interactions serve as the major driving force in the binding of these XO inhibitors. Consistent with our findings, a previous experimental study by Ghallab *et al.* reported that rosmarinic acid is a potent XO inhibitor, with an IC_{50} value of 0.97 μM, supporting the reliability of our calculations (Ghallab et al., 2022). Interestingly, salvianolic acid A showed the strongest binding to XO ($\Delta G_{MM\text{-}PBSA}$ = –83.06 kcal mol^{-1}), surpassing even the reference inhibitor febuxostat ($\Delta G_{MM\text{-}PBSA}$ = –74.96 kcal mol^{-1}). The results demonstrated that the screened compounds represent computationally identified lead molecules for potential XO inhibition. Further *in vitro* experimental studies will be conducted in the future to fully validate these computational findings.

The binding poses of five newly identified XO inhibitors were refined by MD simulations (Fig. 4). Salvianolic acid A formed four HBs with Glu802 and Arg880. Puerarol established three hydrogen bonds (HBs) with Glu802, Gly913, and Glu1261 and π–π interaction with Phe914. Ochnaflavone interacted with Glu802 and Thr1010 through HBs and with Phe649, Phe914, and Phe1009 via π–π stacking. Forsythenside A formed HBs with Glu802, Arg880, and Glu1261, along with π–π interaction with Phe798. Several hydrophobic interactions are observed among the top compounds with residues Leu648, Phe649, Leu873, Ala910, Val1011, Leu1014, Pro1076, and Ala1078. These interactions underscore the importance of hydrogen bonding, π–π stacking, and hydrophobic forces in stabilizing ligand binding.

To gain insight into the interaction of the potential inhibitors with XO, we analyzed the probabilities of HB formation and hydrophobic contacts between the compounds and the protein. The XO residues involved in side-chain (SC) and HB contacts with each inhibitor, based on equilibrated snapshots, are summarized in Table S6 (Supporting Information). Additionally, residues simultaneously forming SC and HB contacts are illustrated in Fig. 5. Notably, key residues such as Leu648, Gln767, Asn768, Lys711, Phe798, Glu802, Leu873, His875, Ser876, Arg880, Ala910, Phe911, Arg912, Gly913, Phe914, Phe1009, Thr1010, Val1011, Phe1013, Leu1014, Pro1076, Ala1078, Ala1079, Ser1080, and Glu1261 were identified as major contributors to ligand binding, highlighting their central role in stabilizing the inhibitor–XO complexes. Notably, previous studies have shown that the catalytic transformation of the purine nucleus by XO involves three key residues, including Glu802, Arg880, and Glu1261, which were also identified in our analysis (Ribeiro et al., 2021).

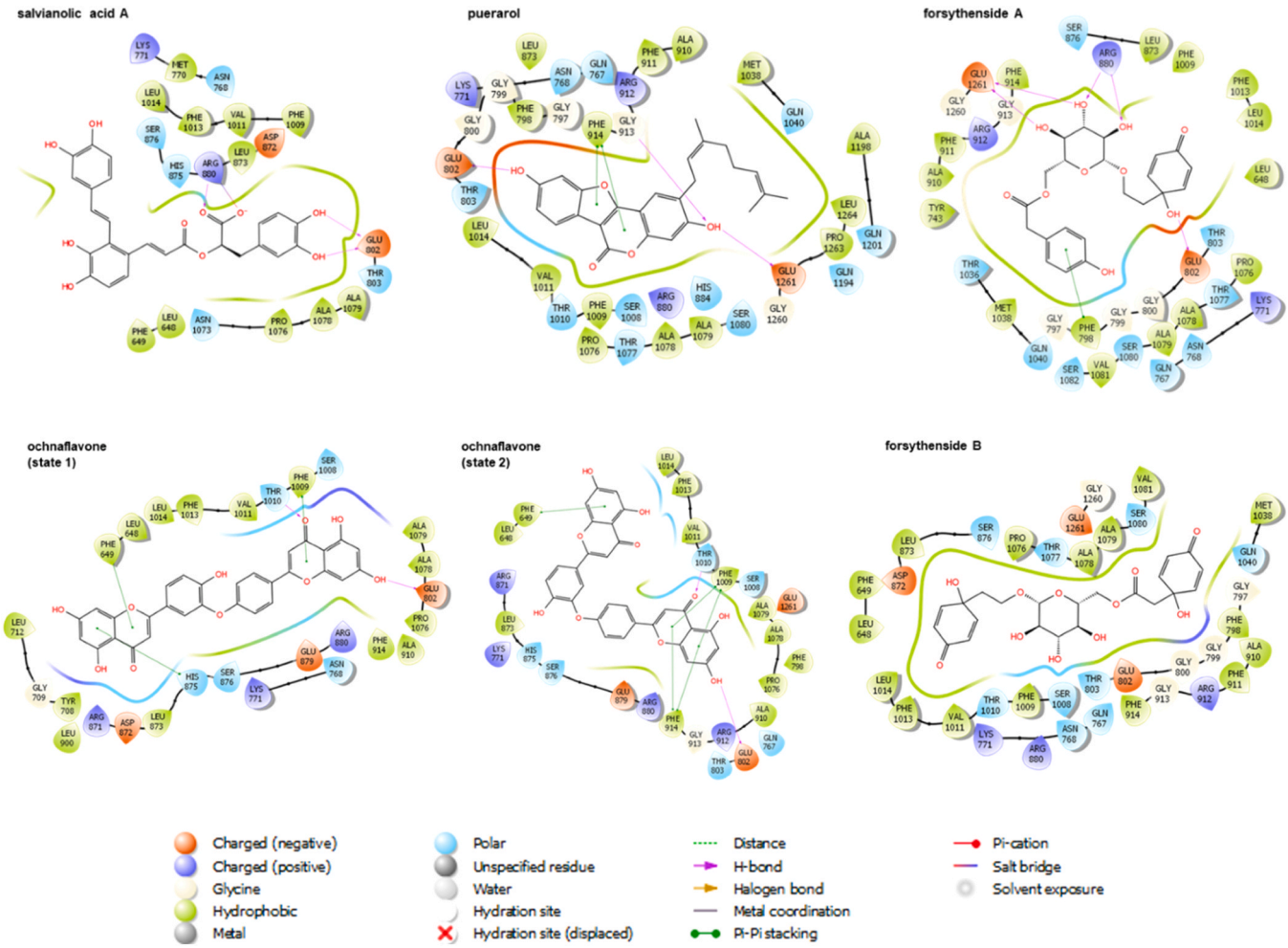

Fig. 4. MD refined structure binding pose between the top compounds and XO protein.

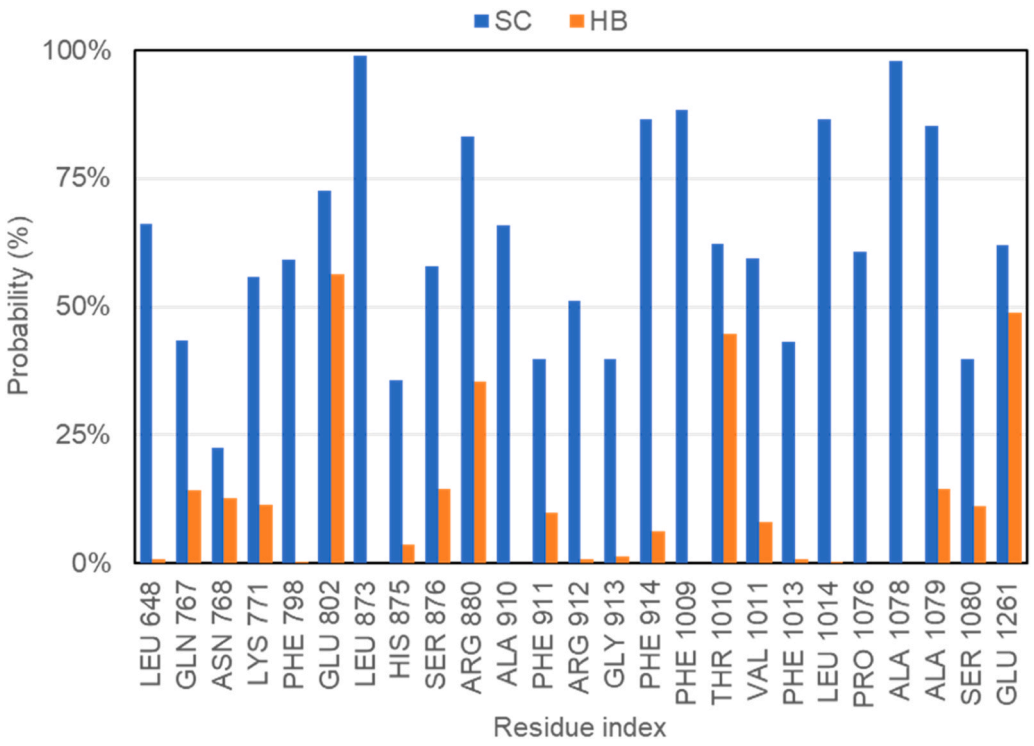

Fig. 5. Probability of forming SC and HB contacts between the top five natural compounds and XO of essential residues. The obtained results were averaged over equilibrated snapshots of MD simulations.

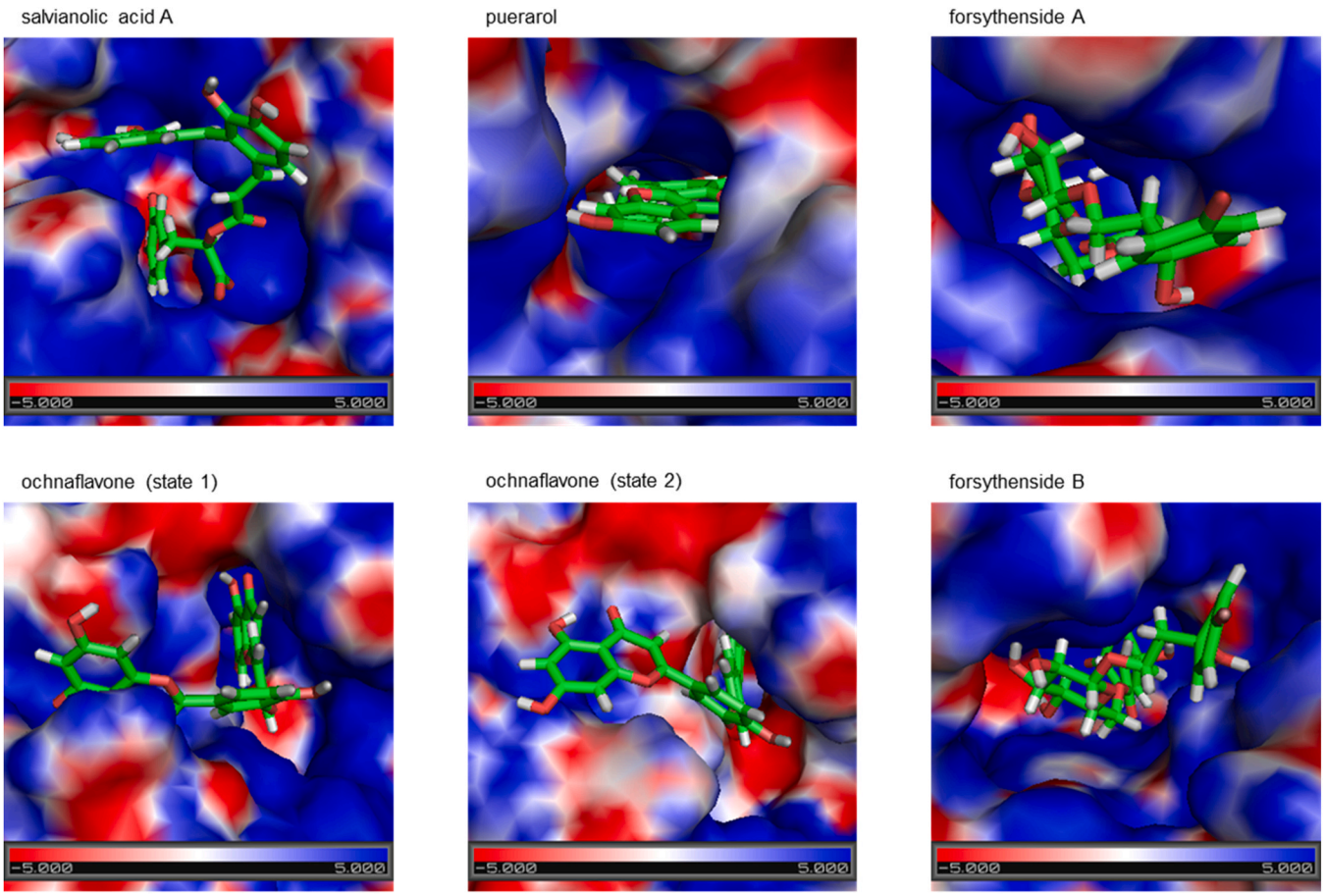

Fig. 6. Electrostatic maps of XO binding pocket in complexes with five potential inhibitors. Red regions represent negative potential areas, and blue regions represent the positive ones.

3.4. Electrostatic analysis of XO complexes

We investigated the electrostatic complementarity of five newly potential inhibitors within the binding site of XO (Fig. 6), using the Adaptive Poisson-Bolzmann Solver (APBS) method (Jurrus et al., 2018). Among the tested ligands, salvianolic acid A exhibited the highest electrostatic compatibility with XO. The binding pocket of XO displayed a strong and localized positive potential that aligned well with the negatively charged carboxylate group of salvianolic acid A, resulting in robust ionic interactions and high binding specificity. A similar result was observed in puerarol, but with a slightly weaker positive potential in the binding pocket. On the other hand, ochnaflavone showed a more balanced distribution of positive and negative areas within the binding pocket, suggesting diverse interaction modes but reduced electrostatic complementarity compared to salvianolic acid A and puerarol. Forsythensides A and B exhibited weaker negative potentials that were either dispersed or gradually distributed, indicating weaker ionic interactions. Consequently, their stability is likely to rely more on non-ionic forces, such as van der Waals or hydrophobic interactions.

3.5. In silico ADME prediction

The evaluation of a potential drug candidate requires systematic investigation of its pharmacokinetic characteristics to ensure adequate penetration and safety within biological systems. Accordingly, an *in silico* prediction of the ADME properties of five newly potential XO inhibitors was performed, and the results are summarized in Table S7, Supporting Information. All compounds, except puerarol, exhibited low BBB values (<1), indicating poor brain penetration, which is consistent with logBB values < 0 for most ligands. Compounds salvianolic acid A, puerarol, and ochnaflavone exhibited certain permeability to Caco2 cells, while all selected derivatives showed high human intestinal absorption (HIA) values, suggesting easy absorption upon oral administration. In addition, all compounds showed no inhibitory or substrate activity toward CYP2D6, a key enzyme involved in the biotransformation of many drugs.

Despite their unfavorable pharmacokinetic properties, the top lead compounds possess core scaffolds with promising XO inhibitory potential and can serve as templates for further structural optimization.

CRediT authorship contribution statement

Anh Hung Nguyen: Investigation, Formal analysis, Data curation. **Anh Tuan Do:** Investigation, Formal analysis, Data curation. **Nguyen Ngoc Linh:** Methodology, Formal analysis. **Minh Quan Pham:** Supervision, Investigation, Data curation. **Son Tung Ngo:** Supervision, Resources, Conceptualization. **Le Thi-Kim Dung:** Writing – review & editing, Writing – original draft, Conceptualization.

Funding

This research was funded by Hanoi Pedagogical University 2 foundation for Sciences and Technology Development via grant number: HPU2.2022-UT-12.

Declaration of Competing Interest

The authors declare that they have no known competing financial interests or personal relationships that could have appeared to influence the work reported in this paper.

Appendix A. Supporting information

Supplementary data associated with this article can be found in the online version at doi:10.1016/j.compbiolchem.2025.108763.

Data availability

Data will be made available on request.

References

Abraham, M.J., Murtola, T., Schulz, R., Páll, S., Smith, J.C., Hess, B., Lindahl, E., 2015. GROMACS: high performance molecular simulations through multi-level parallelism from laptops to supercomputers. SoftwareX 1–2, 19–25. https://doi.org/10.1016/j.softx.2015.06.001.

Aliev, A.E., Kulke, M., Khaneja, H.S., Chudasama, V., Sheppard, T.D., Lanigan, R.M., 2014. Motional timescale predictions by molecular dynamics simulations: case study using proline and hydroxyproline sidechain dynamics. Protein. Struct. Funct. Bioinf 82, 195–215. https://doi.org/10.1002/prot.24350.

Alonso, H., Bliznyuk, A.A., Gready, J.E., 2006. Combining docking and molecular dynamic simulations in drug design. Med. Res. Rev. 26, 531–568. https://doi.org/10.1002/med.20067.

Bayat, S., Aati, O., Rech, J., Sapsford, M., Cavallaro, A., Lell, M., Araujo, E., Petsch, C., Stamp, L.K., Schett, G., Manger, B., Dalbeth, N., 2016. Development of a dual-energy computed tomography scoring system for measurement of urate deposition in gout. Arthritis Care Res. 68, 769–775.

Bell, E.W., Zhang, Y., 2019. DockRMSD: an open-source tool for atom mapping and RMSD calculation of symmetric molecules through graph isomorphism. J. Chemin.. 11, 40–48. https://doi.org/10.1186/s13321-019-0362-7.

Cao, H., Hall, J., Hille, R., 2014a. Substrate orientation and specificity in xanthine oxidase: crystal structures of the enzyme in complex with indole-3-acetaldehyde and guanine. Biochem 53, 533–541. https://doi.org/10.1021/bi401465u.

Cao, H., Pauff, J.M., Hille, R., 2010. Substrate orientation and catalytic specificity in the action of xanthine oxidase: the sequential hydroxylation of hypoxanthine to uric acid. J. Biol. Chem. 285, 28044–28053. https://doi.org/10.1074/jbc.M110.128561.

Cao, H., Pauff, J.M., Hille, R., 2014b. X-ray crystal structure of a xanthine oxidase complex with the flavonoid inhibitor quercetin. J. Nat. Prod. 77, 1693–1699. https://doi.org/10.1021/np500320g.

Case, D.A., Aktulga, H.M., Belfon, K., Cerutti, D.S., Cisneros, G.A., Cruzeiro, V.W.D., Forouzesh, N., Giese, T.J., Götz, A.W., Gohlke, H., Izadi, S., Kasavajhala, K., Kaymak, M.C., King, E., Kurtzman, T., Lee, T.-S., Li, P., Liu, J., Luchko, T., Luo, R., Manathunga, M., Machado, M.R., Nguyen, H.M., O'Hearn, K.A., Onufriev, A.V., Pan, F., Pantano, S., Qi, R., Rahnamoun, A., Risheh, A., Schott-Verdugo, S., Shajan, A., Swails, J., Wang, J., Wei, H., Wu, X., Wu, Y., Zhang, S., Zhao, S., Zhu, Q., Cheatham III, T.E., Roe, D.R., Roitberg, A., Simmerling, C., York, D.M., Nagan, M.C., Merz Jr., K.M., 2023. AmberTools. J. Chem. Inf. Model 63, 6183–6191. https://doi.org/10.1002/prot.24350.

Chhetri, A., Chettri, S., Rai, P., Mishra, D.K., Sinha, B., Brahman, D., 2021. Synthesis, characterization and computational study on potential inhibitory action of novel azo imidazole derivatives against COVID-19 main protease (Mpro: 6LU7). J. Mol. Struct. 1225, 129230–129242. https://doi.org/10.1016/j.molstruc.2020.129230.

Cicero, A.F.G., Fogacci, F., Cincione, R.I., Tocci, G., Borghi, C., 2021. Clinical effects of xanthine oxidase inhibitors in hyperuricemic patients. Med. Princ. Pr. 30, 122–130.

Darden, T., York, D., Pedersen, L., 1993. Particle mesh Ewald: an N·log(N) method for Ewald sums in large systems. J. Chem. Phys. 98, 10089–10092. https://doi.org/10.1159/000512178.

Dong, Y., Huang, H., Zhao, M., Sun-Waterhouse, D., Lin, L., Xiao, C., 2016. Mechanisms underlying the xanthine oxidase inhibitory effects of dietary flavonoids galangin and pinobanksin. J. Funct. Foods 24, 26–36. https://doi.org/10.1016/j.jff.2016.03.021.

Enroth, C., Eger, B.T., Okamoto, K., Nishino, T., Nishino, T., Pai, E.F., 2000. Crystal structures of bovine milk xanthine dehydrogenase and xanthine oxidase: structure-based mechanism of conversion. Proc. Natl. Acad. Sci. 97, 10723–10728. https://doi.org/10.1073/pnas.97.20.10723.

Ghallab, D.S., Shawky, E., Metwally, A.M., Celik, I., Ibrahim, R.S., Mohyeldin, M.M., 2022. Integrated *in silico – in vitro* strategy for the discovery of potential xanthine oxidase inhibitors from Egyptian propolis and their synergistic effect with allopurinol and febuxostat. RSC Adv. 12, 2843–2872. https://doi.org/10.1039/D1RA08011C.

Gliozzi, M., Malara, N., Muscoli, S., Mollace, V., 2016. The treatment of hyperuricemia. Int. J. Cardiol. 213, 23–27. https://doi.org/10.1016/j.ijcard.2015.08.087.

He, Y., Liu, K., Cao, F., Song, R., Liu, J., Zhang, Y., Li, W., Han, W., 2024. Using deep learning and molecular dynamics simulations to unravel the regulation mechanism of peptides as noncompetitive inhibitor of xanthine oxidase. Sci. Rep. 14, 174–185. https://doi.org/10.1038/s41598-023-50686-0.

Huang, S.-Y., Zou, X., 2010. Advances and challenges in protein-ligand docking. Int. J. Mol. Sci. 11, 3016–3034. https://doi.org/10.3390/ijms11083016.

Ishikawa, T., Aw, W., Kaneko, K., 2013. Metabolic interactions of purine derivatives with human ABC Transporter ABCG2: genetic testing to assess gout risk. Pharmaceuticals 6, 1347–1360. https://doi.org/10.3390/ph6111347.

Jurrus, E., Engel, D., Star, K., Monson, K., Brandi, J., Felberg, L.E., Brookes, D.H., Wilson, L., Chen, J., Liles, K., Chun, M., Li, P., Gohara, D.W., Dolinsky, T., Konecny, R., Koes, D.R., Nielsen, J.E., Head-Gordon, T., Geng, W., Krasny, R., Wei, G.W., Holst, M.J., McCammon, J.A., Baker, N.A., 2018. Improvements to the APBS biomolecular solvation software suite. Protein Sci. 27, 112–128. https://doi.org/10.1002/pro.3280.

Kim, S., Thiessen, P.A., Bolton, E.E., Chen, J., Fu, G., Gindulyte, A., Han, L., He, J., He, S., Shoemaker, B.A., Wang, J., Yu, B., Zhang, J., Bryant, S.H., 2016. PubChem Substance and Compound databases. Nucleic Acids Res 44, D1202–D1213. https://doi.org/10.1093/nar/gkv951.

Kolb, P., Irwin, J.J., 2009. Docking screens: right for the right reasons? Curr. Top. Med. Chem. 9, 755–770. https://doi.org/10.2174/156802609789207091.
Kumari, R., Kumar, R., Lynn, A., 2014. g_mmpbsa–a GROMACS tool for high-throughput MM-PBSA calculations. J. Chem. Inf. Model 54, 1951–1962. https://doi.org/10.1021/ci500020m.
Kuntz, I.D., Blaney, J.M., Oatley, S.J., Langridge, R., Ferrin, T.E., 1982. A geometric approach to macromolecule-ligand interactions. J. Mol. Biol. 161, 269–288. https://doi.org/10.1016/0022-2836(82)90153-X.
Kuo, C.-F., Grainge, M.J., Zhang, W., Doherty, M., 2015. Global epidemiology of gout: prevalence, incidence and risk factors. Nat. Rev. Rheuma 11, 649–662. https://doi.org/10.1038/nrrheum.2015.91.
Lee, S.K., G.S.C, Lee, I.H., Chung, J.E., Sung, K.Y., No, K.T., 2004. The PreADME: PC-based program for batch prediction of ADME properties. EuroQSAR 5–10.
Lee, S.K., Lee, I.H., Kim, H.J., Chang, G.S., Chung, J.E., No, K.T., 2003. The PreADME approach: web-based program for rapid prediction of physico-chemical, drug absorption and drug-like properties. EuroQSAR 2002 Designing Drugs and Crop Protectants: Processes, Problems and Solutions. Blackwell Publishing, Maldenh, MA, pp. 418–420. https://doi.org/10.1002/cphc.201701384.
Lipinski, C.A., 2004. Lead- and drug-like compounds: the rule-of-five revolution. Drug Discov. Today Technol. 1, 337–341. https://doi.org/10.1016/j.ddtec.2004.11.007.
Liu, M., Wang, K., Zhang, Y., Zhou, X., Li, W., Han, W., 2025. Mechanistic study of protein interaction with natto inhibitory peptides targeting xanthine oxidase: insights from machine learning and molecular dynamics simulations. J. Chem. Inf. Model 65, 3682–3696. https://doi.org/10.1021/acs.jcim.5c00126.
Maguire, J.B., Boyken, S.E., Baker, D., Kuhlman, B., 2018. Rapid sampling of hydrogen bond networks for computational protein design. J. Chem. Theory Comput. 14, 2751–2760. https://doi.org/10.1021/acs.jctc.8b00033.
Marshall, G.R., 1987. Computer-aided drug design. Annu. Rev. Pharmacol. Toxicol. 27, 193–213. https://doi.org/10.1146/annurev.pa.27.040187.001205.
Masseoud, D., Rott, K., Liu-Bryan, R., Agudelo, C., 2005. Overview of hyperuricaemia and gout. Curr. Pharm. Des. 11, 4117–4124. https://doi.org/10.2174/138161205774913318.
Minh Hoa, T.T., Darmawan, J., Chen, S.L., Van Hung, N., Thi Nhi, C., Ngoc An, T., 2003. Prevalence of the rheumatic diseases in urban Vietnam: a WHO-ILAR COPCORD study. J. Rheuma 30, 2252–2256.
Morris, G.M., Huey, R., Lindstrom, W., Sanner, M.F., Belew, R.K., Goodsell, D.S., Olson, A.J., 2009. AutoDock4 and AutoDockTools4: automated docking with selective receptor flexibility. J. Comput. Chem. 30, 2785–2791. https://doi.org/10.1002/jcc.21256.
Nassar, H., Sippl, W., Dahab, R.A., Taha, M., 2023. Molecular docking, molecular dynamics simulations and in vitro screening reveal cefixime and ceftriaxone as GSK3β covalent inhibitors. RSC Adv. 13, 11278–11290. https://doi.org/10.1039/D3RA01145C.
Ngo, S.T., 2021. Estimating the ligand-binding affinity via λ-dependent umbrella sampling simulations. J. Comput. Chem. 42, 117–123. https://doi.org/10.1002/jcc.26439.
Ngo, S.T., 2022. 501Y.V2 Spike Protein Resists the Neutralizing Antibody in Atomistic Simulations. Comput. Biol. Chem. 97, 107636–107643. https://doi.org/10.1016/j.compbiolchem.2022.107636.
Nguyen, N.T., Nguyen, T.H., Pham, T.N.H., Huy, N.T., Bay, M.V., Pham, M.Q., Nam, P.C., Vu, V.V., Ngo, S.T., 2020. Autodock vina adopts more accurate binding poses but Autodock4 forms better binding affinity. J. Chem. Inf. Model 60, 204–211. https://doi.org/10.1021/acs.jcim.9b00778.
Nguyen, H.A., Nguyen, T.H., Vu, V.V., Derreumaux, P., Ngo, S.T., 2025. Varoglutamstat inhibits the dimerization of the Aβ25–35 fragment in aqueous solution. J. Phys. Chem. B 129, 9304–9311. https://doi.org/10.1021/acs.jpcb.5c03306.
Nguyen, T.H., Tran, P.-T., Pham, N.Q.A., Hoang, V.-H., Hiep, D.M., Ngo, S.T., 2022. Identifying possible AChE inhibitors from drug-like molecules via machine learning and experimental studies. ACS Omega 7, 20673–20682. https://doi.org/10.1021/acsomega.2c00908.
Ojha, R., Singh, J., Ojha, A., Singh, H., Sharma, S., Nepali, K., 2016. An updated patent review: xanthine oxidase inhibitors for the treatment of hyperuricemia and gout (2011-2015). Expert Opin. Ther. Pat. 27, 311–345. https://doi.org/10.1080/13543776.2017.1261111.
Ou, R., Lin, L., Zhao, M., Xie, Z., 2020. Action mechanisms and interaction of two key xanthine oxidase inhibitors in galangal: combination of *in vitro* and *in silico* molecular docking studies. Int. J. Biol. Macromol. 162, 1526–1535. https://doi.org/10.1016/j.ijbiomac.2020.07.297.
Pan, Y., Lu, Z., Li, C., Qi, R., Chang, H., Han, L., Han, W., 2021. Molecular dockings and molecular dynamics simulations reveal the potency of different inhibitors against xanthine oxidase. ACS Omega 6, 11639–11649. https://doi.org/10.1021/acsomega.1c00968.
Parihar, A., Sonia, Z.F., Akter, F., Ali, M.A., Hakim, F.T., Hossain, M.S., 2022. Phytochemicals-based targeting RdRp and main protease of SARS-CoV-2 using docking and steered molecular dynamic simulation: a promising therapeutic approach for Tackling COVID-19. Comput. Biol. Med. 145, 105468–105480. https://doi.org/10.1016/j.compbiomed.2022.105468.
Pascart, T., Lioté, F., 2018. Gout: state of the art after a decade of developments. Rheumatol 27–44. https://doi.org/10.1093/rheumatology/key002.
Pauff, J.M., Cao, H., Hille, R., 2009. Substrate orientation and catalysis at the Molybdenum site in xanthine oxidase. J. Biol. Chem. 284, 8760–8767. https://doi.org/10.1074/jbc.M804517200.
Pauff, J.M., Zhang, J., Bell, C.E., Hille, R., 2008. Substrate orientation in xanthine oxidase: crystal structure of enzyme in reaction with 2-hydroxy-6-methylpurine. J. Biol. Chem. 283, 4818–4824. https://doi.org/10.1074/jbc.M707918200.
Pedley, A.M., Benkovic, S.J., 2017. A new view into the regulation of purine metabolism: the purinosome. Trends Biochem. Sci. 42, 141–154. https://doi.org/10.1016/j.tibs.2016.09.009.
Pham, T.N.H., Nguyen, T.H., Tam, N.M., Y. Vu, T., Pham, N.T., Huy, N.T., Mai, B.K., Tung, N.T., Pham, M.Q., V. Vu, V., Ngo, S.T., 2021. Improving LIgand-ranking of AutoDock vina by changing the empirical parameters. J. Comput. Chem. 43, 160–169. https://doi.org/10.1002/jcc.26779.
Quiroga, R., Villarreal, M.A., 2016. Vinardo: a scoring function based on autodock vina improves scoring, docking, and virtual screening. PLOS One 11, e0155183–e0155200. https://doi.org/10.1371/journal.pone.0155183.
Ribeiro, P.M.G., Fernandes, H.S., Maia, L.B., Sousa, S.F., Moura, J.J.G., Cerqueira, N., 2021. The complete catalytic mechanism of xanthine oxidase: a computational study. Inorg. Chem. Front 8, 405–416. https://doi.org/10.1039/D0QI01029D.
Ryde, U., Soderhjelm, P., 2016. Ligand-binding affinity estimates supported by quantum-mechanical methods. Chem. Rev. 116, 5520–5566. https://doi.org/10.1021/acs.chemrev.5b00630.
Sato, T., Ashizawa, N., Matsumoto, K., Iwanaga, T., Nakamura, H., Inoue, T., Nagata, O., 2009. Discovery of 3-(3-cyano-4-pyridyl)-5-(4-pyridyl)-1,2,4-triazole, FYX-051-a xanthine oxidoreductase inhibitor for the treatment of hyperuricemia. Bioorg. Med. Chem. Lett. 19, 6225–6229. https://doi.org/10.1016/j.bmcl.2009.08.091.
Schrödinger LLC, P., 2010. The PyMOL molecular graphics system. Version 1 (3r1).
Schrödinger LLC, P., 2020. Schrödinger Release 2020-4. Maestro.
Sliwoski, G., Kothiwale, S., Meiler, J., Lowe, E.W., 2014. Computational methods in drug discovery. Pharmacol. Rev. 66, 334–395. https://doi.org/10.1124/pr.112.007336.
Song, J., Wang, Z., Chi, Y., Zhang, Y., Fang, C., Shu, Y., Cui, J., Bai, H., Wang, J., 2023. Anti-gout activity and the interaction mechanisms between Sanghuangporus vaninii active components and xanthine oxidase. Bioorg. Chem. 133, 106394–106403. https://doi.org/10.1016/j.bioorg.2023.106394.
Sousa da Silva, A.W., Vranken, W.F., 2012. ACPYPE - AnteChamber PYthon Parser interfacE. BMC Res. Notes 5, 1–8. https://doi.org/10.1186/1756-0500-5-367.
Tam, N.M., Nguyen, T.H., Pham, M.Q., Hong, N.D., Tung, N.T., Vu, V.V., Quang, D.T., Ngo, S.T., 2023. Upgrading nirmatrelvir to inhibit SARS-CoV-2 Mpro via DeepFrag and free energy calculations. J. Mol. Graph. Model 124, 108535–108541. https://doi.org/10.1016/j.jmgm.2023.108535.
Thai, Q.M., Pham, T.N.H., Hiep, D.M., Pham, M.Q., Tran, P.-T., Nguyen, T.H., Ngo, S.T., 2022. Searching for AChE inhibitors from natural compounds by using machine learning and atomistic simulations. J. Mol. Graph. Model. 115, 108230–108236. https://doi.org/10.1016/j.jmgm.2022.108230.
Thai, Q.M., Phung, H.T.T., Pham, N.Q.A., Horng, J.-T., Tran, P.-T., Tung, N.T., Ngo, S.T., 2024. Natural compounds inhibit Monkeypox virus methyltransferase VP39 in silico studies. J. Biomol. Struct. Dyn. 1–9. https://doi.org/10.1080/07391102.2024.2321509.
Trott, O., Olson, A.J., 2010. Improving the speed and accuracy of docking with a new scoring function, efficient optimization, and multithreading. J. Comput. Chem. 31, 455–461.
Van Drie, J.H., 2007. Computer-aided drug design: the next 20 years. J. Comput. Aided Mol. Des. 21, 591–601. https://doi.org/10.1002/jcc.21334.
Veeresham, C., 2012. Natural products derived from plants as a source of drugs. J. Adv. Pharm. Technol. Res. 3, 200–201. https://doi.org/10.4103/2231-4040.104709.
Wang, W., Kollman, P.A., 2001. Computational study of protein specificity: the molecular basis of HIV-1 protease drug resistance. Proc. Natl. Acad. Sci. 98, 14937–14942. https://doi.org/10.1073/pnas.251265598.
Wang, J., Morin, P., Wang, W., Kollman, P.A., 2001. Use of MM-PBSA in reproducing the binding free energies to HIV-1 RT of TIBO derivatives and predicting the binding mode to HIV-1 RT of efavirenz by docking and MM-PBSA. J. Am. Chem. Soc. 123, 5221–5230. https://doi.org/10.1021/ja003834q.
Wang, J., Wolf, R.M., Caldwell, J.W., Kollman, P.A., Case, D.A., 2004. Development and Testing of a General Amber Force Field. J. Comput. Chem. 25, 1157–1174. https://doi.org/10.1002/jcc.20035.
Wang, Y., Zhang, G., Pan, J., Gong, D., 2015. Novel insights into the inhibitory mechanism of kaempferol on xanthine oxidase. J. Agric. Food Chem. 63, 526–534. https://doi.org/10.1021/jf505584m.
Warren, G.L., Andrews, C.W., Capelli, A.-M., Clarke, B., LaLonde, J., Lambert, M.H., Lindvall, M., Nevins, N., Semus, S.F., Senger, S., 2006. A critical assessment of docking programs and scoring functions. J. Med. Chem. 49, 5912–5931. https://doi.org/10.1021/jm050362n.
Xie, J., Cui, H., Xu, Y., Xie, L., Chen, W., 2021. Delphinidin-3-*O*-sambubioside: a novel xanthine oxidase inhibitor identified from natural anthocyanins. Food Qual. Saf. 5. https://doi.org/10.1093/fqsafe/fyaa038.
Zeng, N., Zhang, G., Hu, X., Pan, J., Zhou, Z., Gong, D., 2018. Inhibition mechanism of baicalein and baicalin on xanthine oxidase and their synergistic effect with allopurinol. J. Funct. Foods 50, 172–182. https://doi.org/10.1016/j.jff.2018.10.005.
Zhang, H., Jiang, Y., Cui, Z., Yin, C., 2018b. Force field benchmark of amino acids. 2. partition coefficients between water and organic solvents. J. Chem. Inf. Model 58, 1669–1681. https://doi.org/10.1021/acs.jcim.8b00493.
Zhang, L., Song, J., Kong, L., Yuan, T., Li, W., Zhang, W., Hou, B., Lu, Y., Du, G., 2020. The strategies and techniques of drug discovery from natural products. Pharmacol. Ther. 216, 107686–107698. https://doi.org/10.1016/j.pharmthera.2020.107686.

Zhang, C., Wang, R., Zhang, G., Gong, D., 2018a. Mechanistic insights into the inhibition of quercetin on xanthine oxidase. Int. J. Biol. Macromol. 112, 405–412. https://doi.org/10.1016/j.ijbiomac.2018.01.190.

Zhang, H., Yin, C., Jiang, Y., van der Spoel, D., 2018c. Force field benchmark of amino acids: i. Hydration and diffusion in different water models. J. Chem. Inf. Model 58, 1037–1052. https://doi.org/10.1021/acs.jcim.8b00026.

Zhang, G., Zhu, M., Liao, Y., Gong, D., Hu, X., 2022. Action mechanisms of two key xanthine oxidase inhibitors in tea polyphenols and their combined effect with allopurinol. J. Sci. Food Agric. 102, 7195–7208. https://doi.org/10.1002/jsfa.12085.